

SURFACE PROPERTIES AND CATALYTIC PERFORMANCE OF Pt/LaSrCoO₄ CATALYSTS IN THE OXIDATION OF HEXANE

Hua Zhong^{1,2*} and Xi-Rui Zeng^{1,2}

¹College of Chemistry and Chemical Engineering, Jinggangshan University, Jian, 343009, PR China

²Provincial Key Laboratory of Coordination Chemistry, Jinggangshan University, Jian, 343009, PR China

(Received May 26, 2006; revised October 1, 2006)

ABSTRACT. Perovskite-type La_{2-x}Sr_xCoO₄ mixed oxides have been prepared by calcination at various temperatures of precipitates obtained from aqueous solutions in the presence of citric or ethylenediaminetetraacetic (EDTA) acids, and have been studied by X-ray diffraction (XRD), surface area (BET) measurements, temperature programmed desorption (TPD), temperature programmed reduction (TPR) and X-ray photoelectron spectroscopy (XPS). These oxides are catalysts for hexane oxidation, with the greatest activity for LaSrCoO₄ calcined at 750 °C. This has extensive oxygen vacancies and large internal surface area. Pt-modified LaSrCoO₄ catalysts are significantly more active than the Pt-free system. Both surface and bulk phases of the perovskite-type oxides contribute to hexane oxidation.

KEY WORDS: Perovskite-type A₂BO₄, Surface properties, Catalytic performance, Temperature programmed desorption (TPD), Temperature programmed reduction (TPR), and X-ray photoelectron spectroscopy (XPS), Hexane oxidation

INTRODUCTION

Volatile organic compounds (VOCs), present in solvents, industrial processes, and combustion products, contribute to atmospheric pollution and are dangerous to human health [1-2]. Their removal is a key topic for research into the protection of the environment. Catalysts based on noble metals (e.g. Pt, Pd) supported on alumina, silica or other oxides have been developed [3-5]. Mixed oxides with the K₂NiF₄ structure, consisting of alternate perovskite (ABO₃) and rock salt (AO) layers, have been examined for their low cost, high catalytic activity and high thermal stability [6]. In A₂BO₄ the B-site is surrounded octahedrally by oxygen and the A-site is in the cavity between these octahedra. Isomorphous replacement allows the physicochemical and catalytic properties to be varied over a wide range. Replacement of A- and/or B-site cations often brings crystal microstrain. Catalytic performance is also associated with variations in the mean valencies of the A- and B-sites [7-10] but detailed investigation is limited and there have been very few reports on three-way catalysts containing noble metals. Further investigation is therefore necessary.

The oxidation reactivity of VOCs is in the following order: alcohols > aldehydes > aromatics > ketones > alkenes > alkanes [11-12]. We have reported investigations of CO and C₃H₈ oxidation over LnSrCoO₄ catalysts (Ln = La, Pr, Nd, Sm, Eu) [13-16], and alkane oxidation represents a good test for activity. The work presented here is a continuation of that in our laboratory and correlates the activity of hexane with that of C₃H₈. A series of catalysts were prepared by thermal decomposition of amorphous citric and ethylene diamine tetraacetic acid complexes and their catalytic activities were investigated by XRD, BET, XPS, TPD and TPR.

*Corresponding author. E-mail: hua_zh@163.com

EXPERIMENTAL

Preparation of catalysts

Lanthanum nitrate, strontium nitrate, cobalt nitrate, EDTA and citric acid were of AR grade purity. Solutions of citric acid, EDTA and ammonia were added to a solution of metal nitrates with La : Sr : Co nominal molar ratio of $2-x : x : 1.0$ ($x = 0.2, 0.4, 0.6, 0.8, 1.0$) at pH 6.5 - 9.5 to form amorphous precipitates in which the ratios of citric acid : EDTA : total metal ions were 1.5 : 1.0 : 1. After evaporation of water at 80 °C, the dark gel was heated at 550 °C for 4 h, pelletized and calcined again at 950, 850 and 750 °C for 10 h.

γ -Al₂O₃ was crushed and sieved to 40 - 60 meshes and calcined overnight at 500 °C. Catalysts with x % LaSrCoO₄/ γ -Al₂O₃, where x wt % is the LaSrCoO₄ content, were prepared by impregnating a γ -Al₂O₃ carrier (surface area, 108.9 m²/g) with an aqueous solution containing the desired molar ratio of lanthanum, strontium, cobalt nitrates and citric acid, followed by drying at 110 °C for 4 h and then calcining at 750 °C in air for 6 h.

γ -Al₂O₃-supported Pt and Pt-modified LaSrCoO₄ catalysts, marked as y % Pt/ γ -Al₂O₃ and y % Pt/LaSrCoO₄, where y wt % is the Pt content were prepared from H₂PtCl₆ using an incipient wetness technique, followed by drying at 110 °C for 4 h and then calcining at 550 °C in air for 6 h. All samples were sieved to this fraction to *ca.* 0.250 - 0.177 mm.

Characterization of catalysts

Phase analysis was performed by X-ray diffraction (D8/ADVANCE, Germany), with Cu K_α radiation. The step scans were taken over the range of 2 θ angles from 20 to 80°. For the evaluations of average crystal size and lattice microstrain of La_{2-x}Sr_xCoO₄, the equations

$$L = 0.9\lambda / \beta \cos \theta$$

and

$$\beta^2 \cos^2 \theta = 4(\lambda/L)^2 / \pi^2 + 32(\epsilon^2) \sin^2 \theta$$

were used: where, L is the average crystal size, λ , the wavelength of the X-ray used (0.154 nm), β , the effective line width of the X-ray reflection, θ , the Bragg angle, and $(\epsilon^2)^{1/2}$, the microstrain density.

The XPS analysis was carried out on a PHI 5000C ESCA spectrometer with Al K_α radiation ($h\nu = 1486.6$ eV). The calcined samples were pressed into small stainless-steel cylinders and outgassed at 10⁻⁵ Pa for 1 h. The residual pressure in the ion-pumped analysis chamber was maintained below 1.3 × 10⁻⁷ Pa during data acquisition. Pretreatments in hydrogen were carried out at 400 °C. Energies were scanned at a pass energy of 20 eV a number of times to obtain good signal to noise ratios. Peak intensities were estimated by calculating the integral of each peak after subtraction of the S-shaped background and fitting to a curve mixed of Lorentzian and Gaussian lines of variable proportion. Although surface charging was observed for all the samples, accurate binding energies (BE) (± 0.2 eV) could be determined by reference to the C_{1s} peak at 284.60 eV.

Specific surface areas (SSA) were calculated by the BET method from nitrogen adsorption isotherms recorded at liquid nitrogen temperature on a Micromeritics apparatus model ST-2000, taking a value of 0.16 nm² for the cross-sectional area of the N₂ molecule adsorbed at -196 °C. Prior to the adsorption measurements samples were outgassed at 130 °C.

TPD measurements were made on an automatic Micromeritics 3000 apparatus interfaced to a data station. Under O₂ gas flow, catalyst samples (300 mg) were heated from ambient temperature to 950 °C at a rate of 8 °C/min and kept at this temperature for 1 h. After the system had cooled to ambient temperature, He carrier gas was used to remove the adsorbed O₂ with a ramp rate of 8 °C/min. The desorption was recorded by a thermal conductor detector (TCD).

The TPR of catalysts was examined with the same apparatus. Since water was produced during reduction, the gases from the reactor were passed through a cold trap before entering the TCD. The samples (100 mg) were first heated to 950 °C at a rate of 20 °C/min in a flow of N₂ (99.9 %) and then cooled to ambient temperature. After being purged by use of 10 % H₂/N₂ for 1 h, with a ramp rate of 20 °C/min, the H₂-reduction was recorded by the TCD.

Activity measurement of catalysts

The catalytic activities (catalyst load 250 mg, particle size 0.250 - 0.177 mm) were measured at atmospheric pressure in an automatic Micromeritics flow reactor. Prior to catalytic tests, the catalysts were treated in an air stream at 500 °C followed by purging in a He stream. For hexane combustion a flow of hexane (1 %) in N₂ mixed with oxygen (10 %) in N₂ (ratio oxygen: hexane = 19.5 : 1 and total Gas Hourly Space Velocity (GHSV) 12000 h⁻¹ was used. The extent of hexane oxidation at 150 - 500 °C was calculated from the C₆H₁₄ and CO₂ content, determined by on-line gas chromatography with a TCD and a Porapak Q column, before and after the reactor. The ambient temperatures for the columns and the TCD were 50 and 75 °C, respectively.

RESULTS AND DISCUSSION

Optimization of La_{2-x}Sr_xCoO₄ catalysts composition and preparation conditions

The XRD patterns of La_{2-x}Sr_xCoO₄ catalysts, displayed in Figure 1, correspond mainly to the perovskite-type structure. However, for La_{2-x}Sr_xCoO₄ catalysts ($x = 0.2$ and 1.0), some diffraction peaks with low intensities were attributed to the La₂O₃ and SrCO₃ phases. A₂BO₄ mixed oxides of K₂NiF₄ structure can be classified into two forms, namely the *F/mmm* orthorhombic-phase and the *I4/mmm* tetragonal-phase, and the *I4/mmm* phase can be classified further into three phases (T, T*, T') [17]. As it is shown in Figure 1, for the La_{2-x}Sr_xCoO₄ catalysts with $x = 0.2$ and 0.4 , only the diffraction peaks attributed to the T phase are observed; while with increasing x weak peaks attributed to the discrete T* phase are also detected. At the same time, the peaks due to the K₂NiF₄ structure phase get stronger and sharper as the calcination temperature increases, indicating an increase in long-range order in the perovskite-type lattice. The lower the calcination temperature, the more the T* phase appears, indicating that there are more oxygen vacancies leading to greater catalytic activity. Table 1 reports the observed values of the lattice parameters, SSAs, calculated metal contents and experimental values from XPS. The experimental and calculated values agree within 5 %. Values of average crystal size and microstrain density are also listed in Table 1. Crystal sizes, L are 153 - 242 Å and decrease as x is increased, whereas the microstrain density decreases. As commonly accepted [18], the microstrain density of the BO₆ unit of A₂BO₄, is a measure of oxygen mobility and the extent to which oxidation is promoted [19].

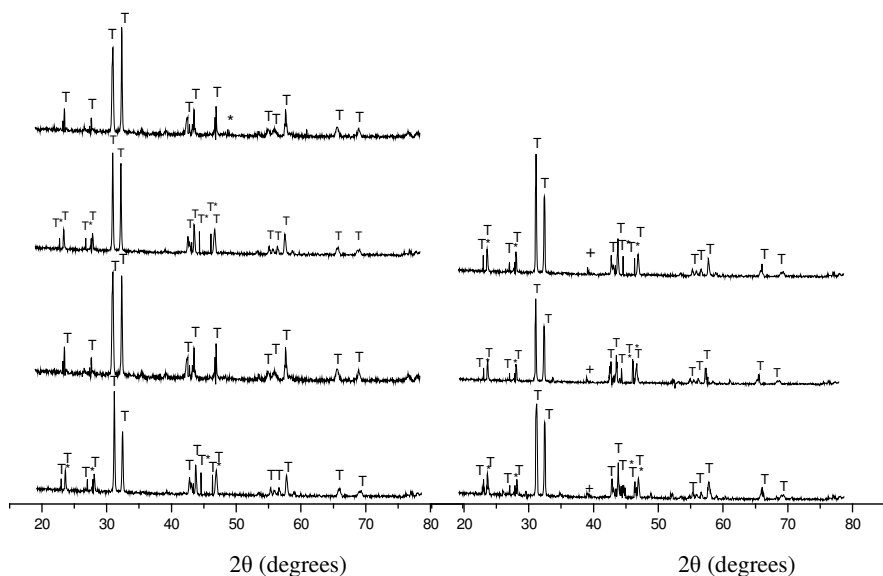


Figure 1. XRD patterns of the $\text{La}_{2-x}\text{Sr}_x\text{CoO}_4$ catalysts T: T phase, T*: T* phase, +: SrCO_3 , * La_2O_3 (a) - (d): $x = 0.2 - 0.8$ (950 °C); (e) - (g): 950, 850, 750 °C ($x = 1.0$).

Table 1. Structure parameter of the $\text{La}_{2-x}\text{Sr}_x\text{CoO}_4$ catalysts.

X in catalyst	Cell parameter			V (\AA^3)	L_{110} (\AA)	$(\epsilon^2)_{110}^{1/2} / 10^3$	S_{BET} (m^2/g)	La content ^a	Sr content	Co content
	A (\AA)	b (\AA)	c (\AA)							
0.2 (950°C)	3.763	3.924	12.836	189.5	241.8	2.55	2.3	64.20(64.15)	4.47(4.49)	15.02(15.04)
0.4 (950°C)	3.769	3.895	12.821	188.2	228.3	2.71	2.4	58.63(58.61)	9.18(9.20)	15.43(15.44)
0.6 (950°C)	3.752	3.923	12.814	188.6	206.7	2.99	2.5	52.74(52.72)	14.16(14.18)	15.87(15.86)
0.8 (950°C)	3.757	3.916	12.837	188.8	190.2	3.25	2.7	46.52(46.55)	19.42(19.40)	16.33(16.36)
1.0 (950°C)	3.759	3.925	12.842	189.5	184.9	3.34	3.1	39.93(39.96)	25.00(25.03)	16.82(16.84)
1.0 (850°C)	3.760	3.902	12.838	188.4	170.1	3.63	3.9	39.93(39.92)	25.00(24.98)	16.82(16.87)
1.0 (750°C)	3.766	3.915	12.799	188.7	153.5	4.02	5.2	39.93(39.89)	25.00(24.97)	16.82(16.90)

V: crystal cell volume; L: average crystalline size; $(\epsilon^2)^{1/2}$: microstrain density; S: specific surface areas; a: metal nominal content, wt.% (experimental values in parentheses).

The TPD profiles (Figure 2.) reveal a large oxygen peak (β) at high temperature (*ca.* 870 °C) for $\text{La}_{2-x}\text{Sr}_x\text{CoO}_4$ catalysts (corresponding to a desorption of $6.8 \times 10^6 \text{ mol O}_2 \text{ m}^{-2}$ for LaSrCoO_4 (750 °C)) and weaker peaks for the other six catalysts. At lower temperature, a broad peak (α) (corresponding to $2.7 \times 10^7 \text{ mol O}_2 \text{ m}^{-2}$ for LaSrCoO_4 (750 °C)) centred at *ca.* 190 °C and a shoulder (α') at *ca.* 315 °C, which may result from desorption of chemically adsorbed oxygen. The desorption peak β , at higher temperature, corresponds to desorption of tightly bound lattice oxygen accompanied by reduction of the transition metal. The α' and β peak areas of LaSrCoO_4 (750 °C) are bigger than those prepared by calcination at other temperatures or with different compositions, implying that there are more oxygen vacancies and mobile lattice oxygen than in the other samples.

The TPR of the sample (described in Table 2) provides information about reducibility of Co^{3+} species in these $\text{La}_{2-x}\text{Sr}_x\text{CoO}_4$ mixed oxides, since both La^{3+} and Sr^{2+} in A-sites are not reduced under the conditions employed. The hydrogen uptake by TPR at low temperature is due to the

reduction of over-stoichiometric and adsorbed oxygen as well as the reduction of Co³⁺ to Co²⁺, and the samples still preserve the K₂NiF₄-type structure as a whole. The hydrogen uptake at high temperature is ascribed to the reduction of Co²⁺ to Co⁰, which leads to the breakdown of the K₂NiF₄-type structure and formation of the discrete phases La₂O₃, La(OH), La(OH)₃, SrO, and Co. The H₂ consumed at low temperature ranges from 0.325 to 0.492 mol H₂ (mol Co)⁻¹. The observed unit cell expansion is explained by oxidation from Co²⁺ to Co³⁺ inside the perovskite structure, which in order to preserve charge neutrality, becomes more oxygen-deficient. The H₂ consumption at higher temperature varies from 1.018 to 1.035 mol H₂ (mol Co)⁻¹, indicating little change in the Co³⁺ and Co²⁺ content.

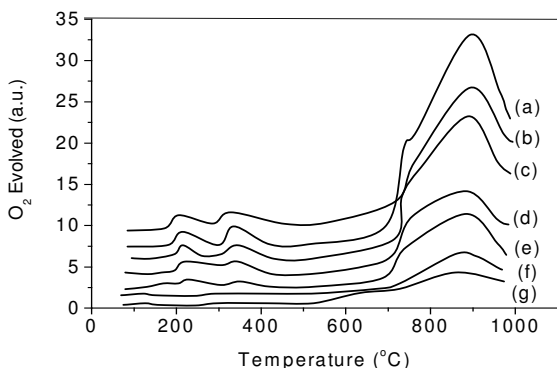


Figure 2. TPD patterns of the La_{2-x}Sr_xCoO₄ catalysts (a) - (c): 750, 850, 950 °C (x = 1.0), (d) - (g): x = 0.2 - 0.8 (950 °C)

The above results indicate that the catalytic activity for the oxidation of hexane (see Table 2) is closely related to the surface area and the oxygen deficiency of the catalyst. The LaSrCoO₄ (750 °C) catalyst displayed relatively good catalytic activity for the total oxidation of hexane, and was thus selected as the host catalyst for modification by platinum in the following work.

Table 2. Physico-chemical characteristics of the La_{2-x}Sr_xCoO₄ catalysts.

X in catalyst	H _{2low T} (mol H ₂ mol ⁻¹ Co)	H _{2high T} (mol H ₂ mol ⁻¹ Co)	Co ³⁺ /Co _{tot} (mol mol ⁻¹)	RR (mmol g ⁻¹ h ⁻¹)	SRR (mmol m ⁻² h ⁻¹)
0.2 (950 °C)	0.325	1.024	0.581	0.83	0.36
0.4 (950 °C)	0.338	1.027	0.596	0.89	0.37
0.6 (950 °C)	0.356	1.019	0.612	1.03	0.41
0.8 (950 °C)	0.403	1.018	0.645	1.24	0.46
1.0 (950 °C)	0.434	1.034	0.668	1.77	0.57
1.0 (850 °C)	0.456	1.035	0.672	2.69	0.69
1.0 (750 °C)	0.492	1.033	0.684	4.32	0.83

H_{2low T}: hydrogen uptake by TPR at low T, H_{2high T}: hydrogen uptake by TPR at high T, Co³⁺/Co_{tot}: ratio determined by TPR H₂ uptake, RR: reaction rate at 320 °C, SRR: surface reaction rate at 320 °C.

Catalytic activities for the oxidation of hexane of the Pt-modified LaSrCoO₄-based catalysts

All the samples were tested in the catalytic combustion of hexane. Carbon dioxide and water were the only products. As both Sr²⁺ and La³⁺ ions tend to be carbonated when kept at ambient temperatures for long periods, synthesised samples can display variable amounts of carbonate.

In order to diminish the effect of this surface contamination on the catalyst performance, a cleaning procedure was applied as described in the experimental section. Results for the oxidation of hexane over a series of Pt/LaSrCoO₄ catalysts and related systems are summarized in Table 3. By comparing the 50 % and 99 % conversion temperatures (T_{50} , T_{99}) of the Pt-doped and Pt-free systems, it is evident that the incorporation of platinum into the LaSrCoO₄ catalyst improved the catalyst performance. The T_{50} and T_{99} of the 0.3 % Pt/LaSrCoO₄ catalyst decreased from 258 and 342 °C in the Pt-free systems to 227 and 269 °C, respectively, in the doped materials. In addition, the C₆H₁₄ conversion increased initially with increasing wt % Pt, and was optimum with 0.3 wt % Pt for the LaSrCoO₄ catalyst prepared by calcination at 750 °C. The conversion of C₆H₁₄ over all these γ -Al₂O₃-supported LaSrCoO₄ systems was lower than that of the unsupported 100 % LaSrCoO₄ system. Moreover, the conversion of C₆H₁₄ increased with LaSrCoO₄-loading although the surface area decreased greatly because the γ -Al₂O₃ surface area, 108.9 m²/g, is bigger than that of LaSrCoO₄. This implies that both the surface and the bulk perovskite play important roles in the catalytic oxidation of hexane.

Table 3. Catalytic behavior for hexane oxidation over Pt/LaSrCoO₄ catalysts and related systems.

Catalyst	T ₅₀ (°C)	T ₉₉ (°C)
10 % LaSrCoO ₄ /γ-Al ₂ O ₃	325	486
20 % LaSrCoO ₄ /γ-Al ₂ O ₃	302	434
25 % LaSrCoO ₄ /γ-Al ₂ O ₃	279	398
33 % LaSrCoO ₄ /γ-Al ₂ O ₃	261	367
100 % LaSrCoO ₄	258	342
0.05 % Pt/LaSrCoO ₄	253	335
0.1 % Pt/LaSrCoO ₄	247	318
0.2 % Pt/LaSrCoO ₄	240	296
0.3 % Pt/LaSrCoO ₄	227	269
0.5 % Pt/LaSrCoO ₄	239	294
0.3 % Pt/γ-Al ₂ O ₃	236	277

Characterization of the Pt-modified LaSrCoO₄-based catalysts

By contrast with the LaSrCoO₄ catalyst (see Figure 3 a.), the XRD patterns of the three Pt-modified LaSrCoO₄ catalysts (see Figure 3 b, c and d) show besides the features ascribed to the perovskite structure two weak peaks at $2\theta = 26.05$ and 42.70 that become more pronounced as the Pt percentage increases from 0.1 to 0.5 %. These can be attributed to crystallites of PtCl₄ by comparison with the known 2θ values for PtCl₄. In addition, for the 0.3 % Pt/LaSrCoO₄ and 0.5 % Pt/LaSrCoO₄ catalysts, the peaks at 39.80, 46.30 and 67.55 could be assigned to the Pt metallic phase. However, there is no conclusive evidence for the existence of Pt crystallites on the catalyst of 0.1 % Pt-modified LaSrCoO₄.

The results of O₂-TPD investigation (Figure 4) show that differences between the doped and undoped catalysts in their adsorption/desorption behavior towards oxygen. Comparing with Pt-free LaSrCoO₄, the 0.3 % Pt/LaSrCoO₄ catalyst shows stronger peaks at 80 and 220 °C, which are evidently related to the doping of H₂PtCl₆ in LaSrCoO₄. However, the peaks at 200, 315 and over 600 °C for the two catalysts are very similar in position and intensity, and so originate from desorption of the same kind of strongly adsorbed oxygen. Therefore the O₂-TPD results indicate that the doping of H₂PtCl₆ in the LaSrCoO₄ catalyst leads to enhancement of oxygen adsorption and of species able to participate in the oxidation of hexane.

The TPR profiles of the LaSrCoO₄ and 0.3 % Pt/LaSrCoO₄ catalysts are displayed in Figure 5. For the 0.3 % Pt/LaSrCoO₄ catalyst, the reduction profile consists of four sets of peaks and there is another peak at 130 °C, which could be attributed to reduction of PtO₂ [20]. At the same time,

the high temperature (810 °C) reduction peak, which leads to the breakdown of the perovskite-type phase, is unchanged in position and shape. However, the shift of the low temperature reduction peaks at 290 and 410 °C to lower temperatures suggests that doping by Pt improves the low temperature reducibility of the perovskite-type LaSrCoO₄.

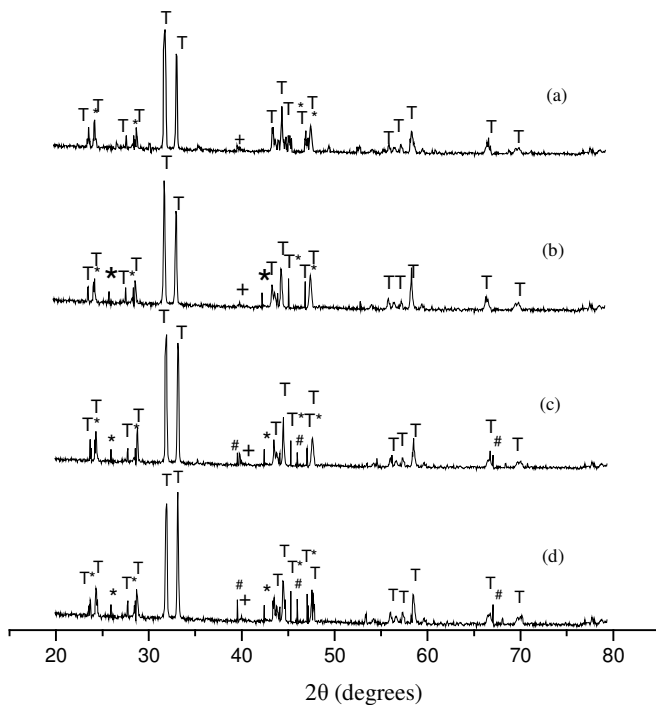


Figure 3. XRD patterns of the catalysts T: T phase, T*: T* phase, +: SrCO₃, *: PtCl₄, #: Pt. a: LaSrCoO₄; b: 0.1 % Pt/LaSrCoO₄; c: 0.3 % Pt/LaSrCoO₄; d: 0.5 % Pt/LaSrCoO₄.

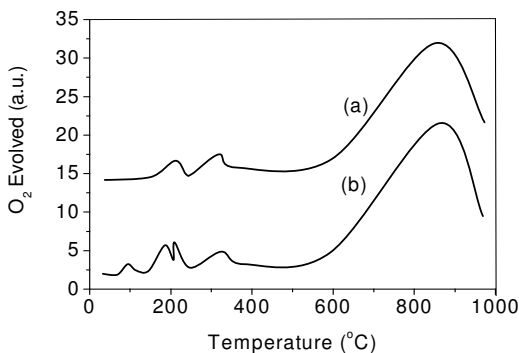


Figure 4. TPD patterns of the catalysts (a): LaSrCoO₄; (b): 0.3 % Pt/LaSrCoO₄.

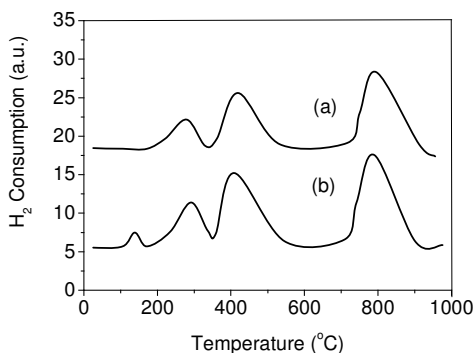


Figure 5. TPR patterns of the catalysts (a): LaSrCoO₄; (b): 0.3 % Pt/LaSrCoO₄.

Table 4 lists the corresponding binding energies for La_{3d5/2}, Co_{2p3/2}, Sr_{3d5/2} and O_{1s} of the LaSrCoO₄ and 0.3 % Pt/LaSrCoO₄ catalysts, together with the molar percentage of cations of the three component elements on the surface [21]. Table 4 shows that the binding energy for La_{3d5/2} is the same for the two samples, which indicates that the doping Pt does not appear to affect to a significant extent the binding energy of La_{3d5/2} level. The XPS spectra of Co_{2p} display signals at 780.8 and 795.5 eV, which can be ascribed to Co²⁺(2p) and Co³⁺(2p), respectively [22]. The value for Co³⁺ for 0.3 % Pt/LaSrCoO₄ catalyst is greater than that of the LaSrCoO₄ catalyst, indicating that the surface concentration of Co³⁺ increases after the doping with H₂PtCl₆. However, the Co/(La+Sr) surface ratios are much higher than expected, suggesting that Co cations are enriched on the surface. The surface concentration of Co for 0.3 % Pt/LaSrCoO₄ catalyst is bigger than that of the LaSrCoO₄ catalyst. The O_{1s} results show that there are two signals, with the binding energy *ca.* 529.0 and 531.1 eV, assigned to lattice oxygen and oxygen adsorbed as O⁻ or OH⁻, respectively [23]. The intensity of the O_{1s} signal of 0.3 % Pt/LaSrCoO₄ at 529.0 eV is bigger than that of LaSrCoO₄. Since the 531.1 eV signal of O_{1s} is attributed to chemically adsorbed oxygen, there are probably more oxygen vacancies in 0.3 % Pt/LaSrCoO₄ than there are in LaSrCoO₄. The Pt (4f)-XPS spectra of the Pt/LaSrCoO₄ catalysts are shown in Figure 6, in which the peaks at 75.5 eV and 71.2 eV are assigned to Pt⁰ [24] and PtCl₄⁻, respectively. As the peak at 71.2 eV is strengthened as the % Pt increases from 0.3 to 0.5, we suggest that most of the Pt species on the surface layer of the Pt-doped LaSrCoO₄ system is Pt⁴⁺.

Table 4. XPS La_{3d}, Sr_{3d}, Co_{2p} and O_{1s} binding energies and surface compositions of catalysts.

Catalyst	XPS-BE (eV) ^a				Surface molar (%)			Co/(La+Sr) (mol/mol)
					La	Sr	Co	
LaSrCoO ₄	834.8	133.7	779.1	528.9	31.8	32.4	35.8	0.56
			795.2	531.0				
0.3%Pt/LaSrCoO ₄	834.9	133.8	778.9	529.2	30.5	31.3	38.2	0.62
			795.7	531.5				

^aCalibrated internally by the carbon deposit C_{1s} at 284.60eV (BE).

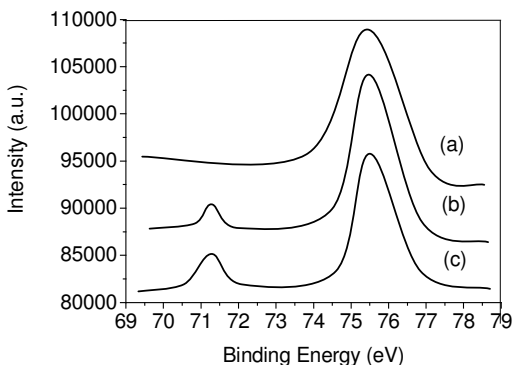


Figure 6. XPS patterns of Pt_{4f} of the catalysts (a) - (c): 0.1 %, 0.3 %, 0.5 % (Pt/LaSrCoO₄).

ACKNOWLEDGEMENTS

This work was supported by the Science and Technology Bureau of Jian, Jiangxi Province of China (Project No. 20052817). The authors greatly appreciated discussions with the group working on this project.

REFERENCES

1. Kosouko, M.; Nunez, C.M. *J. Air Waste Manage. Assoc.* **1990**, *40*, 254.
2. Dimitriadis, B. *Metal Finishing* **1997**, *95*, 55.
3. Baldwin, T.R.; Burch, R. *Appl. Catal. A: Gen.* **1995**, *66*, 339.
4. Lyubovski, M.; Pfefferle, L. *Catal. Today* **1999**, *47*, 29.
5. Garbowski, E.; Labalme, V.; Benhamon, N.; Guillaume, N.; Primet, M. *Appl. Catal. A: Gen.* **1995**, *133*, 351.
6. Peter, S.D.; Garbowski, E.; Guillaume, N.; Perrichon, V.; Primet, M. *Catal. Lett.* **1998**, *54*, 79.
7. Liu, Y.; Yang, X.G.; Liu, Y.M.; Wu, Y. *Acta Phy-chem. Sin.* **1999**, *15*, 506.
8. Gao, L.Z.; Au, C.T. *Catal. Lett.* **2000**, *65*, 91.
9. Wu, Y.; Zhao, Z.; Liu, Y.; Yang, X. *J. Mol. Catal. A: Chemical* **2000**, *155*, 89.
10. Ladavos, A.K.; Pomonis, P.J. *Appl. Catal. A: Gen.* **1997**, *165*, 73.
11. Hermia, J.; Vigneron, S. *Catal. Today* **1993**, *17*, 349.
12. Malley, A.O.; Hodnett, B.K. *Catal. Today* **1999**, *54*, 31.
13. Yang, X.M.; Luo, L.T.; Zhong, H. *Appl. Catal. A: Gen.* **2004**, *272*, 299.
14. Luo, L.T.; Zhong, H.; Yang, X.M. *J. Serb. Chem. Soc.* **2004**, *69*, 783.
15. Yang, X.M.; Luo, L.T.; Zhong, H. *React. Kine. Catal. Lett.* **2004**, *81*, 219.
16. Yang, X.M.; Luo, L.T.; Zhong, H. *Catal. Communications* **2005**, *6*, 13.
17. Tokura, Y.; Takagi, H.; Uchida, S. *Nature* **1989**, *337*, 345.
18. Liu, Y.; Yang, X.G.; Liu, Y.M.; Wu, Y. *Acta Phys.-chim. Sin.* **1999**, *15*, 506.
19. Gao, L. Z.; Dong, B. L.; Li, Q. S.; Lu, X.; Yu, Z. L.; Wu, Y. *J. Fuel. Chem. Tech.* **1994**, *22*, 113.
20. Huizinga, T.; Grondelle, J.; Prins, R. *Appl. Catal. B: Environmental* **1984**, *10*, 199.

21. Wagner, C.D.; Davis, L.E.; Zeller, M.V.; Taylor, J.A.; Raymond, R.H.; Gale, L.H. *Surf. Interface Anal.* **1981**, 3, 211.
22. Olamoto, Y.; Imanaka, T. *Appl. Catal. B: Environmental* **1991**, 73, 249.
23. He, H.; Dai, H.X.; Au, C.T. *Appl. Catal. B: Environmental* **1997**, 33, 65.
24. Yu, Y.T.; Xu, B.Q. *Acta Chem. Sin.* **2003**, 61, 1758.